



This is a repository copy of *Contrasting effects of energy transfer in determining efficiency improvements in ternary polymer solar cells*.

White Rose Research Online URL for this paper:

<https://eprints.whiterose.ac.uk/125492/>

Version: Published Version

---

**Article:**

Li, W., Yan, Y., Gong, Y. et al. (7 more authors) (2018) Contrasting effects of energy transfer in determining efficiency improvements in ternary polymer solar cells. *Advanced Functional Materials*, 28 (5). 1704212. ISSN 1616-301X

<https://doi.org/10.1002/adfm.201704212>

---

This is the peer reviewed version of the following article: W. Li, Y. Yan, Y. Gong, J. Cai, F. Cai, R. S. Gurney, D. Liu, A. J. Pearson, D. G. Lidzey, T. Wang, *Adv. Funct. Mater.* 2017, 1704212, which has been published in final form at <https://doi.org/10.1002/adfm.201704212>. This article may be used for non-commercial purposes in accordance with Wiley Terms and Conditions for Self-Archiving.

**Reuse**

This article is distributed under the terms of the Creative Commons Attribution (CC BY) licence. This licence allows you to distribute, remix, tweak, and build upon the work, even commercially, as long as you credit the authors for the original work. More information and the full terms of the licence here:

<https://creativecommons.org/licenses/>

**Takedown**

If you consider content in White Rose Research Online to be in breach of UK law, please notify us by emailing [eprints@whiterose.ac.uk](mailto:eprints@whiterose.ac.uk) including the URL of the record and the reason for the withdrawal request.



[eprints@whiterose.ac.uk](mailto:eprints@whiterose.ac.uk)  
<https://eprints.whiterose.ac.uk/>

# Contrasting Effects of Energy Transfer in Determining Efficiency Improvements in Ternary Polymer Solar Cells

Wei Li, Yu Yan, Yanyan Gong, Jinlong Cai, Feilong Cai, Robert S. Gurney, Dan Liu, Andrew J. Pearson, David G. Lidzey, and Tao Wang\*

Crystallizable, high-mobility conjugated polymers have been employed as secondary donor materials in ternary polymer solar cells in order to improve device efficiency by broadening their spectral response range and enhancing charge dissociation and transport. Here, contrasting effects of two crystallizable polymers, namely, PffBT4T-2OD and PDPP2TBT, in determining the efficiency improvements in PTB7-Th:PC<sub>71</sub>BM host blends are demonstrated. A notable power conversion efficiency of 11% can be obtained by introducing 10% PffBT4T-2OD (relative to PTB7-Th), while the efficiency of PDPP2TBT-incorporated ternary devices decreases dramatically despite an enhancement in hole mobility and light absorption. Blend morphology studies suggest that both PffBT4T-2OD and PDPP2TBT are well dissolved within the host PTB7-Th phase and facilitate an increased degree of phase separation between polymer and fullerene domains. While negligible charge transfer is determined in binary blends of each polymer mixture, effective energy transfer is identified from PffBT4T-2OD to PTB7-Th that contributes to an improvement in ternary blend device efficiency. In contrast, energy transfer from PTB7-Th to PDPP2TBT worsens the efficiency of the ternary device due to inefficient charge dissociation between PDPP2TBT and PC<sub>71</sub>BM.

## 1. Introduction


Over the past ten years, promising progress has been made in organic photovoltaics (OPVs) by developing new electron donors

W. Li, Y. Yan, Y. Gong, J. Cai, F. Cai, Dr. R. S. Gurney, Dr. D. Liu, Prof. T. Wang  
State Key Laboratory of Silicate Materials for Architectures  
Wuhan University of Technology  
Wuhan 430070, China  
E-mail: twang@whut.edu.cn

W. Li, Y. Yan, Y. Gong, J. Cai, F. Cai, Dr. R. S. Gurney, Dr. D. Liu, Prof. T. Wang  
School of Materials Science and Engineering  
Wuhan University of Technology  
Wuhan 430070, China

Dr. A. J. Pearson  
Cavendish Laboratory  
University of Cambridge  
J. J. Thomson Avenue, Cambridge CB3 0HE, UK

Prof. D. G. Lidzey  
Department of Physics and Astronomy  
University of Sheffield  
Sheffield S3 7RH, UK

 The ORCID identification number(s) for the author(s) of this article can be found under <https://doi.org/10.1002/adfm.201704212>.

© 2017 The Authors. Published by WILEY-VCH Verlag GmbH & Co. KGaA, Weinheim. This is an open access article under the terms of the Creative Commons Attribution License, which permits use, distribution and reproduction in any medium, provided the original work is properly cited.

DOI: 10.1002/adfm.201704212

and acceptors,<sup>[1,2]</sup> controlling and optimizing the nanoscale morphology,<sup>[3–5]</sup> and via interfacial engineering of the device architectures.<sup>[6,7]</sup> Power conversion efficiency (PCE) metrics for this technology now stand at 13% for lab-scale single junction and tandem devices.<sup>[8,9]</sup> Ternary photovoltaic blends,<sup>[10–15]</sup> prepared by incorporating a third component into the donor:acceptor active layer, have emerged as a promising strategy for realizing further improvements in PCE by enhancing device spectral response and charge collection efficiency. This method is favorable as it removes the time-consuming and expensive process of synthesizing new conjugated polymers, in addition to the complicated manufacturing steps that are associated with tandem solar cell fabrication.<sup>[16,17]</sup>

Recent work has shown that semi-crystalline conjugated macromolecules or small molecules are effective third components when preparing efficient ternary solar cells.<sup>[18–20]</sup> For example,

both the crystallinity and face-on preferential polymer orientation in PTB7-Th:PC<sub>71</sub>BM binary blends can be simultaneously enhanced via the addition of a highly crystalline small molecule *p*-DTS(FBTTH<sub>2</sub>)<sub>2</sub>, resulting in a high PCE of 10.5% (a relative improvement of 14%).<sup>[21]</sup> Elsewhere, the incorporation of Si-PCDTBT into the PTB7:PC<sub>71</sub>BM system can result in high device fill factors (FF; up to 77%) through a significant reduction in charge recombination within the active layer.<sup>[22]</sup> Although these crystallizable additives can be highly ordered in relatively simple pure and binary systems, their ability to undergo ordering in ternary blends is not always realized.<sup>[23]</sup> Their exact location within the ternary blend morphology—and the corresponding impacts on charge dissociation and transport—has not been fully explored and understood due to the fact that interactions and intermixing in three material systems is considerably more complicated to analyze than in two material systems. In addition to photocurrent generation from two independent cells, charge and energy transfer between the electron donor or acceptor and the third component can also occur in ternary cells.<sup>[24]</sup> The complexity of this case encourages the comprehensive understanding and control of photocurrent generation to rationally prepare ternary OPVs with high performance.

Poly([2,6'-4,8-di(5-ethylhexylthienyl)benzo[1,2-b;3,3'-b']dithiophene]{3-fluoro-2[(2-ethylhexyl)carbonyl]thieno[3,4-b]thiophenediyl}) (PTB7-Th) is a new benchmark electron-donating

polymer, which can achieve high photovoltaic efficiency when combined with [6,6]-phenyl C<sub>71</sub> butyric acid methyl ester (PC<sub>71</sub>BM) in OPVs. However, its inferior hole mobility and poor crystallinity limited the further improvement of device performance. Poly[(5,6-difluoro-2,1,3-benzothiadiazol-4,7-diyl)-alt-(3,3''-di(2-octyldodecyl)2,2';5',2'';5'',2''''-quaterthiophen-5,5''''-diyl)] (PffBT4T-2OD) and poly[2,5-(2-octyldodecyl)-3,6-diketopyrrolopyrrole-alt-5,5''-(2,5-di(thien-2-yl)thieno[3,2-b]thiophene)] (PDPP2TBT) are two kinds of crystallizable conjugated polymers with high hole mobility. Introducing them as a secondary donor into PTB7-Th:PC<sub>71</sub>BM system should bring the possibility to promote ideal morphology and improve hole mobility to obtain higher PCE. In this work, we have studied the PffBT4T-2OD- and PDPP2TBT-based ternary solar cells and demonstrated two contrasting effects that determine the efficiency changes in their respective systems. At the macroscopic level, the addition of an optimum amount of PffBT4T-2OD leads to improvement in PCE from 10.3% for the binary device to 11.0% for the ternary device, while the addition of PDPP2TBT always led to a reduction. Morphology studies indicate that these secondary donors locate within the host polymer (PTB7-Th) and increase the sizes of polymer- and fullerene-rich domains. While negligible charge transfer can be observed in binary blends of polymer mixtures, effective energy transfer was identified from PffBT4T-2OD to PTB7-Th that lead to improved device efficiency, and from PTB7-Th to PDPP2TBT which deteriorated the efficiency of the ternary device due to inefficient charge dissociation between PDPP2TBT and PC<sub>71</sub>BM. Our results suggest that energy transfer is a critical factor that should be prioritized when incorporating crystallizable, high mobility conjugated polymers as ternary components in photovoltaic blends to improve device efficiency.

## 2. Results and Discussion

The energy level diagrams and chemical structures of PTB7-Th, PDPP2TBT, PffBT4T-2OD, and PC<sub>71</sub>BM are shown in Figure 1a,b.<sup>[23,25,26]</sup> Figure 1c,d shows the thin-film absorption spectra of these materials, PTB7-Th:PC<sub>71</sub>BM binary blends and ternary blends with various concentrations of PffBT4T-2OD and PDPP2TBT. It can be seen that PTB7-Th shows strong absorption between 550 and 780 nm while PC<sub>71</sub>BM shows strong absorption below 550 nm. The PTB7-Th:PC<sub>71</sub>BM binary film shows broadband absorption across the visible region, consistent with the high PCE values (above 10%) seen in various device studies.<sup>[27,28]</sup> PffBT4T-2OD also exhibits strong absorption from 500 to 740 nm, thereby offering a boost to the absorption efficiency of PTB7-Th:PC<sub>71</sub>BM binary films within its existing range. PDPP2TBT, on the other hand, has its strongest absorption between 750 and 900 nm, consequently the absorption efficiency of PTB7-Th:PC<sub>71</sub>BM is significantly extended into the near-IR upon its introduction. Based upon this data alone one would therefore predict a higher potential photocurrent in PDPP2TBT-based ternary devices compared to PffBT4T-2OD-based ternary devices.

In order to test this prediction, ternary solar cells were fabricated with both conventional (indium-tin-oxide (ITO)/poly(3,4-ethylenedioxythiophene):poly(styrene sulfonate)

(PEDOT:PSS)/Active layer/Ca/Ag) and inverted (ITO/electron transport layer (ETL)/Active layer/MoO<sub>3</sub>/Ag) architectures. The ETL in our inverted device architecture utilizes a TiO<sub>2</sub>/titanium oxide bis(2,4-pentanedionate) (TOPD) layer which was formed after thermal annealing of a TiO<sub>2</sub>/titanium(diisopropoxide) bis(2,4-pentanedionate) (TIPD) layer, and have been demonstrated as an efficient ETL for organic and perovskite photovoltaics in our previous work.<sup>[27,29]</sup> The weight ratio of electron donors (i.e., PTB7-Th and PffBT4T-2OD or PDPP2TBT) to PC<sub>71</sub>BM was fixed at 1:1.5, and each active layer thickness was maintained at ≈100 nm according to a previous study.<sup>[30,31]</sup> Typical *J*-*V* curves for the two groups of inverted ternary OPVs are illustrated in Figure 1e, with the corresponding PCE metrics summarized in Table 1. Device data for conventional-architecture ternary OPVs is presented in Table S1 (Supporting Information) in the Supporting Information. Our inverted ternary OPVs demonstrated superior device performance compared with the conventional devices, however both type of devices showed the same trends with regards to PffBT4T-2OD and PDPP2TBT incorporation. For inverted devices, reference PTB7-Th:PC<sub>71</sub>BM OPV gave a maximum PCE of 10.3% (average PCE 10.2 ± 0.09%), with an open-circuit voltage (*V*<sub>oc</sub>) of 0.79 V, a short-circuit current density (*J*<sub>sc</sub>) of 18.2 mA cm<sup>-2</sup>, and an FF of 71.4%. Over the composition range investigated (i.e., up to 20 wt%), the *V*<sub>oc</sub> of the PffBT4T-2OD-based ternary OPVs reduced slightly, a result that is consistent with a previous report.<sup>[23]</sup> However, both *J*<sub>sc</sub> and FF increased and led to an overall enhancement in PCE. An optimum PffBT4T-2OD content was identified to be 10 wt% (corresponding to an active layer component ratio of PTB7-Th:PffBT4T-2OD:PC<sub>71</sub>BM of 0.9:0.1:1.5), which increased the *J*<sub>sc</sub> from 18.2 to 18.6 mA cm<sup>-2</sup>, FF from 71.4% to 75.7%, and maximum PCE from 10.3% to 11.0%. Literature work on PTB7-Th:PC<sub>71</sub>BM-based ternary solar cells have reported improved PCEs via the increase in *J*<sub>sc</sub>.<sup>[14,32,33]</sup> However, the improved PCE in this work mainly resulted from the increase of FF from 71.4% to 75.7%, which is among the highest FF in PTB7-Th-based ternary bulk heterojunction (BHJ) solar cells (see a literature survey of Table S2, Supporting Information). With the addition of more PffBT4T-2OD, device PCE started to decrease due to reductions in FF and *V*<sub>oc</sub>. Similar to the PffBT4T-2OD-based ternary OPVs, the *V*<sub>oc</sub> of the PDPP2TBT-based ternary OPVs was also reduced by adding the same wt%, albeit to a larger extent.

The *V*<sub>oc</sub> of some ternary solar cells have been found to be fixed to the smallest difference between the highest occupied molecular orbital (HOMO) energy levels of the donors and the lowest unoccupied molecular orbital (LUMO) energy levels of the acceptors,<sup>[34-36]</sup> whereas other research also reported that the *V*<sub>oc</sub> of ternary devices can change linearly with the addition content of the third component.<sup>[37-39]</sup> In this work, the *V*<sub>oc</sub> of the PTB7-Th:PC<sub>71</sub>BM, PffBT4T-2OD:PC<sub>71</sub>BM, and PDPP2TBT:PC<sub>71</sub>BM conventional binary OPVs were determined to be 0.80, 0.77, and 0.68 V, respectively (see Table S1, Supporting Information), and the *V*<sub>oc</sub> of our ternary devices lies between the *V*<sub>oc</sub> values of corresponding binary solar cells, and changed correspondingly by compositional changes in our ternary blends.<sup>[40,41]</sup> In contrast to the enhanced *J*<sub>sc</sub> and FF in PffBT4T-2OD-based ternary OPVs, both *J*<sub>sc</sub> and FF decreased dramatically in PDPP2TBT-based ternary OPVs. For example, after adding 20 wt% PDPP2TBT (corresponding to a ratio of

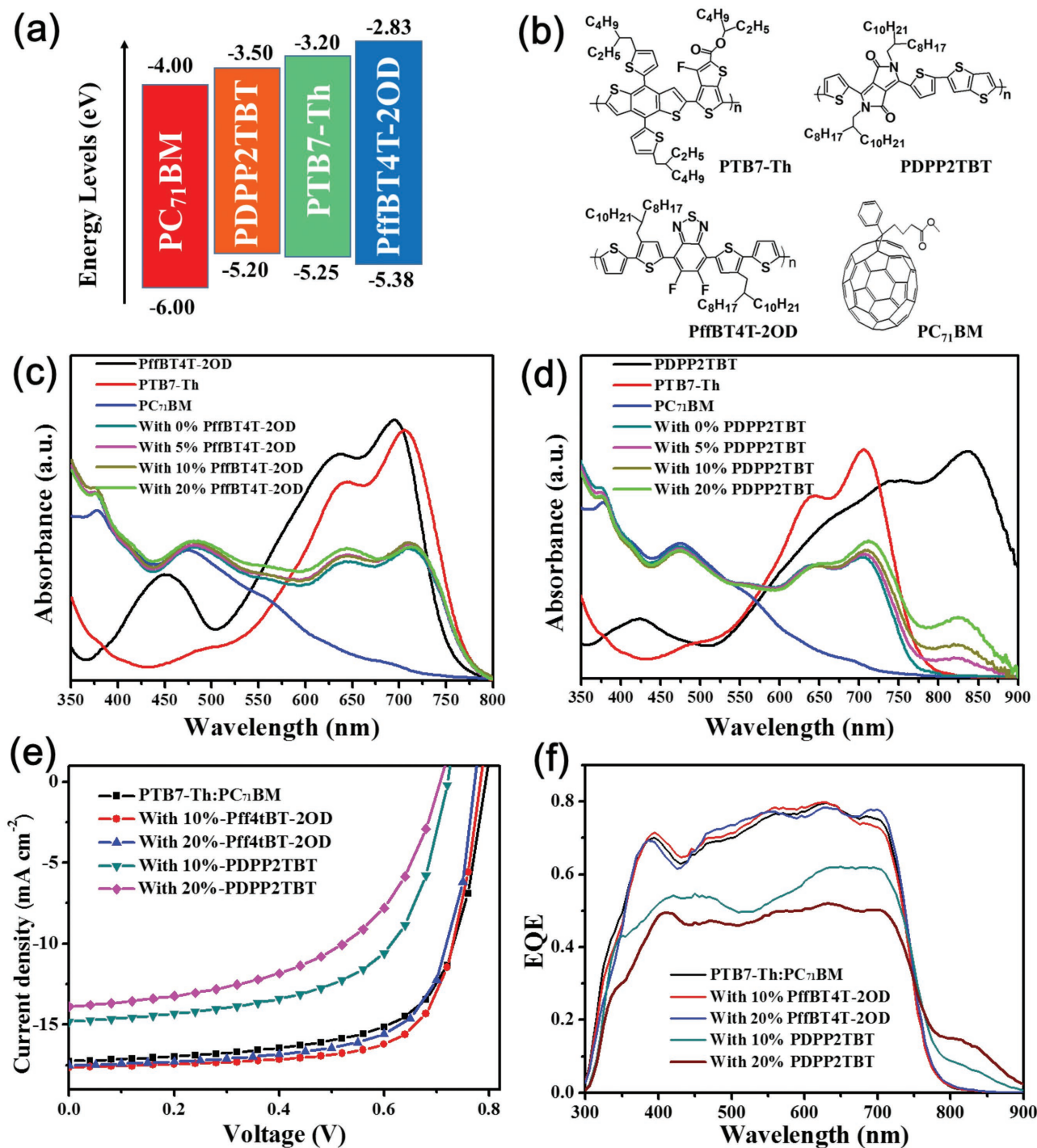


**Figure 1.** a) The energy levels and b) chemical structures of PTB7-Th, PDPP2TBT, PffBT4T-2OD, and PC<sub>71</sub>BM. c,d) The absorption spectra of PTB7-Th, PffBT4T-2OD, PDPP2TBT, PC<sub>71</sub>BM, and PTB7-Th:PC<sub>71</sub>BM blends with different amount of PffBT4T-2OD or PDPP2TBT contents. e) Champion *J*-*V* curves of inverted ternary organic solar cells with different contents of PffBT4T-2OD and PDPP2TBT. The weight ratio of electron-donating polymer to PC<sub>71</sub>BM was fixed at 1:1.5. f) Corresponding EQE spectra.

PTB7-Th:PDPP2TBT:PC<sub>71</sub>BM of 0.8:0.2:1.5), the ternary OPVs exhibited a low maximum PCE of 5.25% and 5.57% in conventional and inverted devices, respectively. External quantum efficiency (EQE) measurements were carried out to characterize the spectral response range and magnitude of each solar cell

type. As shown in Figure 1f, the EQE of PffBT4T-2OD-based ternary OPVs is marginally higher than the reference device, in line with the weak increase in *J*<sub>sc</sub> observed through *J*-*V* measurements. For PDPP2TBT-based ternary OPVs the enhanced spectral response above 800 nm (cf. blend film absorption

**Table 1.** Summary of photovoltaic parameters of inverted ternary solar cells with different contents of PffBT4T-2OD and PDPP2TBT under the illumination of AM1.5G at  $100 \text{ mW cm}^{-2}$ . The data presented are the maximum values followed with average values and standard deviations in the parentheses obtained from over 20 individual devices.

	$V_{oc}$ [V]	$J_{sc}$ [ $\text{mA cm}^{-2}$ ]	FF [%]	PCE [%]
PTB7-Th:PC <sub>71</sub> BM	0.79 (0.79 ± 0.002)	18.2 (18.1 ± 0.32)	71.4 (71.3 ± 0.63)	10.31 (10.20 ± 0.09)
With 5% PffBT4T-2OD	0.78 (0.78 ± 0.002)	18.3 (18.2 ± 0.47)	73.7 (72.8 ± 0.54)	10.60 (10.55 ± 0.08)
With 10% PffBT4T-2OD	0.78 (0.78 ± 0.005)	18.6 (18.2 ± 0.42)	75.7 (75.5 ± 0.23)	11.00 (10.85 ± 0.21)
With 15% PffBT4T-2OD	0.78 (0.78 ± 0.003)	18.5 (18.2 ± 0.45)	74.8 (74.2 ± 0.11)	10.86 (10.79 ± 0.11)
With 20%-PffBT4T-2OD	0.77 (0.77 ± 0.001)	18.4 (18.3 ± 0.42)	73.9 (73.5 ± 0.40)	10.59 (10.57 ± 0.18)
With 5%-PDPP2TBT	0.75 (0.74 ± 0.003)	16.4 (15.8 ± 0.40)	62.3 (61.0 ± 0.30)	7.66 (7.53 ± 0.13)
With 10%-PDPP2TBT	0.73 (0.72 ± 0.005)	15.6 (15.5 ± 0.63)	61.6 (60.2 ± 0.20)	6.98 (6.86 ± 0.13)
With 15%-PDPP2TBT	0.72 (0.71 ± 0.002)	14.6 (14.4 ± 0.43)	59.4 (59.2 ± 0.20)	6.22 (6.17 ± 0.12)
With 20%-PDPP2TBT	0.71 (0.70 ± 0.002)	14.1 (13.2 ± 0.53)	55.3 (54.3 ± 0.40)	5.57 (5.23 ± 0.15)

data in Figure 1d) is greatly offset by the reduced EQE at wavelengths below 750 nm. Although both PffBT4T-2OD and PDPP2TBT are semi-crystalline polymers with high structural order and carrier mobility,<sup>[42,43]</sup> our device study demonstrates two contrasting effects in the ternary OPVs: a moderate amount of PffBT4T-2OD can increase the efficiency of ternary OPV through primary improvement in device FF, whereas PDPP2TBT deteriorates the device performance significantly despite the potential for higher absorption efficiency.

To understand these contrasting effects in determining device efficiency, the active layer morphology was first explored. **Figure 2** shows bright-field transmission electron microscopy (TEM) images of relevant binary and ternary thin films, in which the dark and bright regions represent the fullerene

and polymer domains, respectively, due to their different electron densities.<sup>[44]</sup> It can be seen from Figure 2a that the PTB7-Th:PC<sub>71</sub>BM blend film exhibits a homogeneous distribution of donor and acceptor, indicating good mixing between PTB7-Th and PC<sub>71</sub>BM. While this nanostructure is beneficial for charge dissociation, it may limit charge transport and extraction efficiencies due to the lack of a well-defined bicontinuous network. Both PDPP2TBT:PC<sub>71</sub>BM and Pff4TBT-2OD:PC<sub>71</sub>BM blend films comprise fibril-like structures that we identify as semi-crystalline polymer domains (seen in Figure 2d,e). With the introduction of PDPP2TBT or PffBT4T-2OD into the host blend, the bright and dark areas become more distinct, suggesting higher degrees of phase separation within the ternary active layers. Surface topography characterization via scanning probe

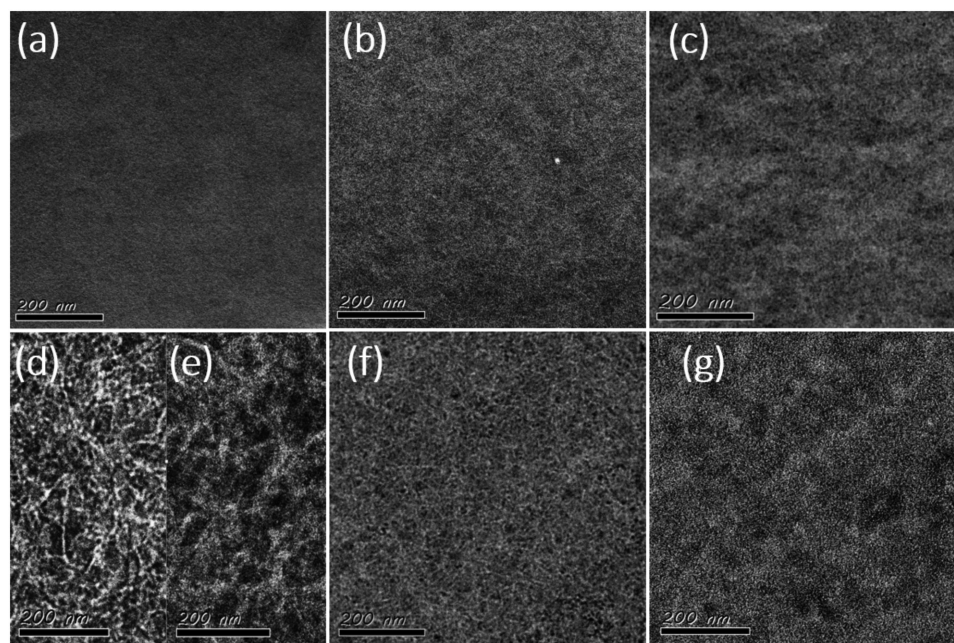


**Figure 2.** TEM images of the binary and ternary films: a) PTB7-Th:PC<sub>71</sub>BM; b) PTB7-Th:PffBT4T-2OD:PC<sub>71</sub>BM (0.9:1:1.5); c) PTB7-Th:PffBT4T-2OD:PC<sub>71</sub>BM (0.8:0.2:1.5); d) PffBT4T-2OD:PC<sub>71</sub>BM (1:1.5); e) PDPP2TBT:PC<sub>71</sub>BM (1:1.5); f) PTB7-Th:PDPP2TBT:PC<sub>71</sub>BM (0.9:0.1:1.5); g) PTB7-Th:PDPP2TBT:PC<sub>71</sub>BM (0.8:0.2:1.5).

microscopy (SPM) suggests that all ternary blend films are smooth with a low root-mean-square roughness (up to 2.2 nm, data presented in Figure S1, Supporting Information). However, with the addition of an excessive amount of the third component (i.e., 20 wt%), pronounced phase separation takes place which would likely reduce the efficiency of free charge generation due to the reduced donor:acceptor interfacial area. The observed trends of morphological evolution are consistent with the device data discussed earlier. To verify that the bright areas in the ternary blends are consistent with a nanostructure comprised of well-mixed polymer domains, rather than the existence of crystalline fibril-like polymers (which would also increase the contrast in the TEM images), grazing incidence wide-angle X-ray scattering (GIWAXS) measurements were performed on the PffBT4T-2OD-based ternary blend series as these show a positive impact on device efficiency. From the GIWAXS patterns shown in Figure S2a,b (Supporting Information) we find that PTB7-Th and PffBT4T-2OD form face-on  $\pi$ - $\pi$  stacking and edge-on crystalline lamellae, respectively, in their pure films. However, with the addition of up to 20 wt% PffBT4T-2OD explored in this work, the 2D GIWAXS patterns of the ternary blend films (Figure S2d-f, Supporting Information) have only minor

changes compared with the binary PTB7-Th:PC<sub>71</sub>BM blend film (Figure S2c, Supporting Information). As the PffBT4T-2OD (h00) lamellar diffraction peaks are absent in Figure S2d-f (Supporting Information), we can conclude that the PffBT4T-2OD component is in a largely amorphous state after being incorporated into the PTB7-Th:PC<sub>71</sub>BM blend. Our observation agrees with the previous conclusion that the PffBT4T-2OD component only crystallizes when its wt% in the PTB7-Th:PC<sub>71</sub>BM blend is 50% or higher, however the efficiency of the ternary device has deteriorated by more than half at this loading.<sup>[23]</sup>

We performed further grazing incidence small-angle X-ray scattering (GISAXS) measurements to quantify domain size changes in the ternary blend films. 2D GISAXS patterns are shown in Figure 3a-g for binary PTB7-Th:PC<sub>71</sub>BM blend films, and ternary films with 5%, 10%, or 20% of PDPP2TBT or PffBT4T-2OD. The 1D profiles at the specular beam position within the region  $q_z = 0.03 \pm 0.002 \text{ \AA}^{-1}$  are plotted in Figure 3h,i. The profiles were fitted with a universal model (described in detail in the Supporting Information).<sup>[45]</sup> The fitting parameters are shown in Table 2, where  $\xi$  is the average correlation length of the polymer phase,  $\eta$  and  $D$  are the correlation length and dimensionality of the fractal-like network of PC<sub>71</sub>BM clusters,

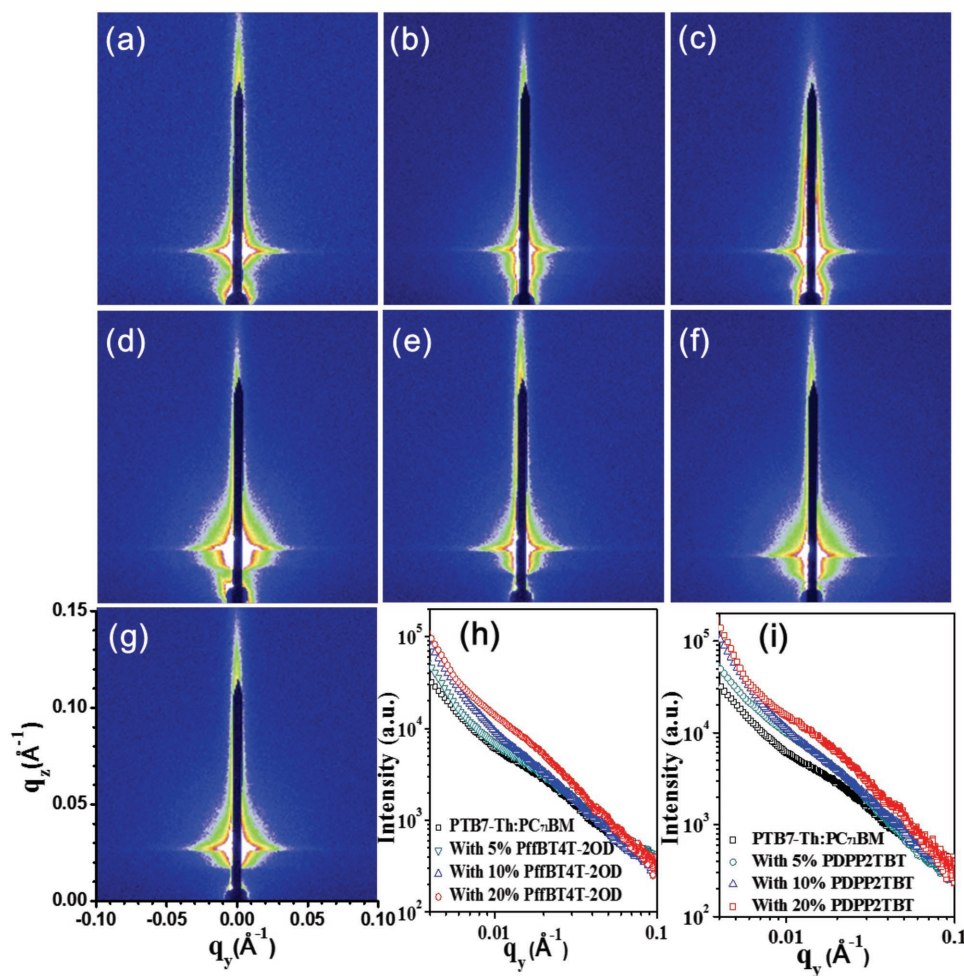


**Figure 3.** 2D GISAXS patterns of a) PTB7-Th:PC<sub>71</sub>BM, and its ternary blends with b) 5%, c) 10%, and d) 20% PffBT4T-2OD; e) 5%, f) 10%, and g) 20% PDPP2TBT. 1D GISAXS profiles along  $q_y$  axis for PTB7-Th:PC<sub>71</sub>BM blend films with differing amounts of h) PffBT4T-2OD or i) PDPP2TBT.

**Table 2.** Fitting parameters of 1D GISAXS profiles for PTB7-Th:PC<sub>71</sub>BM binary and ternary films.

	$\xi$ [nm]	$\eta$ [nm]	$D$	$2R_g$ [nm]
PTB7-Th:PC <sub>71</sub> BM	27.1	7.5	2.05	26.4
5% PffBT4T-2OD	36.3	8.1	2.10	30.2
10% PffBT4T-2OD	40.6	9.0	2.10	32.4
20% PffBT4T-2OD	49.1	10.8	2.05	38.0
5% PDPP2TBT	32.4	11.6	2.00	40.0
10% PDPP2TBT	42.7	12.5	2.00	43.2
20% PDPP2TBT	94.8	13.7	1.80	43.4

respectively.  $2R_g$  is the product of  $\eta$  and  $D$ , which represents the length of the clustered PC<sub>71</sub>BM domain (Guinier radius). The binary PTB7-Th:PC<sub>71</sub>BM film showed the smallest correlation length of polymer (27.1 nm) and clustered PC<sub>71</sub>BM (26.4 nm) domains, in line with literature reports.<sup>[46,47]</sup> In both ternary blends  $\xi$  and  $2R_g$  become larger, indicating an increase in phase separation between polymer- and fullerene-rich domains and providing independent confirmation of the trends observed from TEM. Despite the enlargement in polymer and fullerene domain size in the ternary blends, the fractal dimension for all blends is around 2, suggesting that fullerene packing is comparably loose (i.e., relatively diffuse interfaces), consistent with a morphology that enables both efficient exciton dissociation and charge transport.<sup>[48]</sup>

Surface energy differences between materials is believed to act as a strong driving force for determining the localization of the third component in ternary blends.<sup>[49]</sup> The localization of PDPP2TBT and PffBT4T-2OD in the ternary blends was inferred from surface energy analysis (details described in the Supporting Information). As summarized in Table S5 (Supporting Information), the wetting coefficient of PDPP2TBT and PffBT4T-2OD in PTB7-Th:PC<sub>71</sub>BM were 1.76 and 1.85, respectively, indicating PDPP2TBT and PffBT4T-2OD are both located within PTB7-Th domains.<sup>[50]</sup>

We proceeded to evaluate exciton dissociation and charge carrier recombination and transport in the binary and ternary blend devices. Figure S4a (Supporting Information) shows the photocurrent density ( $J_{ph}$ ) as a function of the effective voltage ( $V_{eff}$ )

**Table 3.**  $J_{sat}$ ,  $P(E,T)$  and hole mobility in binary and ternary OPVs.

	$J_{sat}$ [mA cm <sup>-2</sup> ]	$P(E,T)$ [%]	Hole mobility [cm <sup>2</sup> V <sup>-1</sup> s <sup>-1</sup> ]
PTB7-Th:PC <sub>71</sub> BM	19.0	95.5	$3.5 \times 10^{-4}$
With 5% PffBT4T-2OD	19.1	96.5	$1.2 \times 10^{-3}$
With 10% PffBT4T-2OD	19.0	97.4	$2.5 \times 10^{-3}$
With 15% PffBT4T-2OD	19.1	96.7	$3.6 \times 10^{-3}$
With 20% PffBT4T-2OD	19.0	96.5	$4.1 \times 10^{-3}$
With 5% PDPP2TBT	17.0	96.7	$2.1 \times 10^{-3}$
With 10% PDPP2TBT	16.2	96.2	$3.2 \times 10^{-3}$
With 15% PDPP2TBT	15.3	95.4	$4.3 \times 10^{-3}$
With 20% PDPP2TBT	15.0	93.3	$6.3 \times 10^{-3}$

of our binary and ternary devices. The  $J_{ph}$  of all devices saturates when  $V_{eff}$  is around 1 V, indicating that all photogenerated electron–hole pairs are dissociated under this condition. The saturated short-circuit current density ( $J_{sat}$ ) of PffBT4T-2OD-based ternary OPVs are roughly constant at 19.0 mA cm<sup>-2</sup> across the concentration series. The  $J_{sat}$  of PDPP2TBT-based ternary OPVs however decreased with the addition of PDPP2TBT. As the value of  $J_{sat}$  reflects how many excitons are generated by the absorbed incident photons, and is limited by the maximum exciton generation rate,<sup>[51]</sup> our results suggest that the exciton generating process is unchanged with the addition of PffBT4T-2OD. Conversely, the process is hampered by the addition of PDPP2TBT despite its ability to enhance absorption efficiency. This behavior can be quantified further by calculating the charge collection probability  $P(E,T)$ , found by normalizing  $J_{ph}$  with respect to  $J_{sat}$  ( $J_{ph}/J_{sat}$ ). **Table 3** shows  $P(E,T)$  values for our various ternary OPVs under short circuit conditions. It can be seen that the  $P(E,T)$  values of PffBT4T-2OD-based ternary OPVs are all higher than those of the baseline PTB7-Th:PC<sub>71</sub>BM binary OPV, and a maximal value of 97.4% is achieved with 10% PffBT4T-2OD. However, for PDPP2TBT-based OPVs,  $P(E,T)$  decreases with increasing amounts of PDPP2TBT, indicating that the addition of this polymer has a negative effect on charge dissociation. Related studies have shown that the hole mobility of pure PDPP2TBT and PffBT4T-2OD can reach at 10 and 10<sup>-2</sup> cm<sup>2</sup> V<sup>-1</sup> s<sup>-1</sup>, respectively.<sup>[25,52]</sup> The hole mobility in our films, calculated using dark  $J-V$  data (Figure S4b, Supporting Information) and SCLC theory, supports the notion that these component additives in the PTB7-Th:PC<sub>71</sub>BM binary OPVs enhances the hole mobility, from 10<sup>-4</sup> to 10<sup>-3</sup> cm<sup>2</sup> V<sup>-1</sup> s<sup>-1</sup>. Hole mobility therefore cannot explain the contrasting phenomenon in device efficiency changes in these two groups of ternary OPVs.

In order to evaluate any charge transfer between the third component and PTB7-Th in the blend host, a series of binary solar cells were fabricated using PTB7-Th:Pff4TBT-2OD and PTB7-Th:PDPPP2TBT as the active layer. The  $J-V$  curves of these binary devices were measured under AM1.5G illumination at 100 mW cm<sup>-2</sup> and are shown in **Figure 4a,b**. It is apparent that these binary solar cells show a much lower  $J_{sc}$  value than solar cells with PC<sub>71</sub>BM as the acceptor. The devices with a pure layer of PDPP2TBT, PffBT4T-2OD, and PTB7-Th only obtained a  $J_{sc}$  of 0.02, 0.25, and 0.65 mA cm<sup>-2</sup>, respectively, as a result of charge dissociation at the interface with the cathode. For the PTB7-Th:PDPP2TBT binary solar cells, the  $J_{sc}$  values are located between the  $J_{sc}$  values of PTB7-Th and PDPP2TBT, illustrating that the exciton dissociation at the PTB7-Th:PDPP2TBT interfaces is negligible and therefore there is no charge transfer between them. Such behavior is also present in the PTB7-Th:PffBT4T-2OD binary devices, so it can be concluded that no charge transfer takes place between each polymer:polymer combination.

As discussed in previous studies,<sup>[24,53,54]</sup> overlap between the emission spectrum of one material and the absorption spectrum of another material is a requirement for efficient Förster-type energy transfer. Figure S5a,b (Supporting Information) and Figure 4c,d show the absorption and photoluminescence (PL) spectra of PffBT4T-2OD, PTB7-Th, PDPP2TBT, PTB7-Th:PffBT4T-2OD binary, and PTB7-Th:PDPP2TBT binary films. It can be seen that the maximum absorption

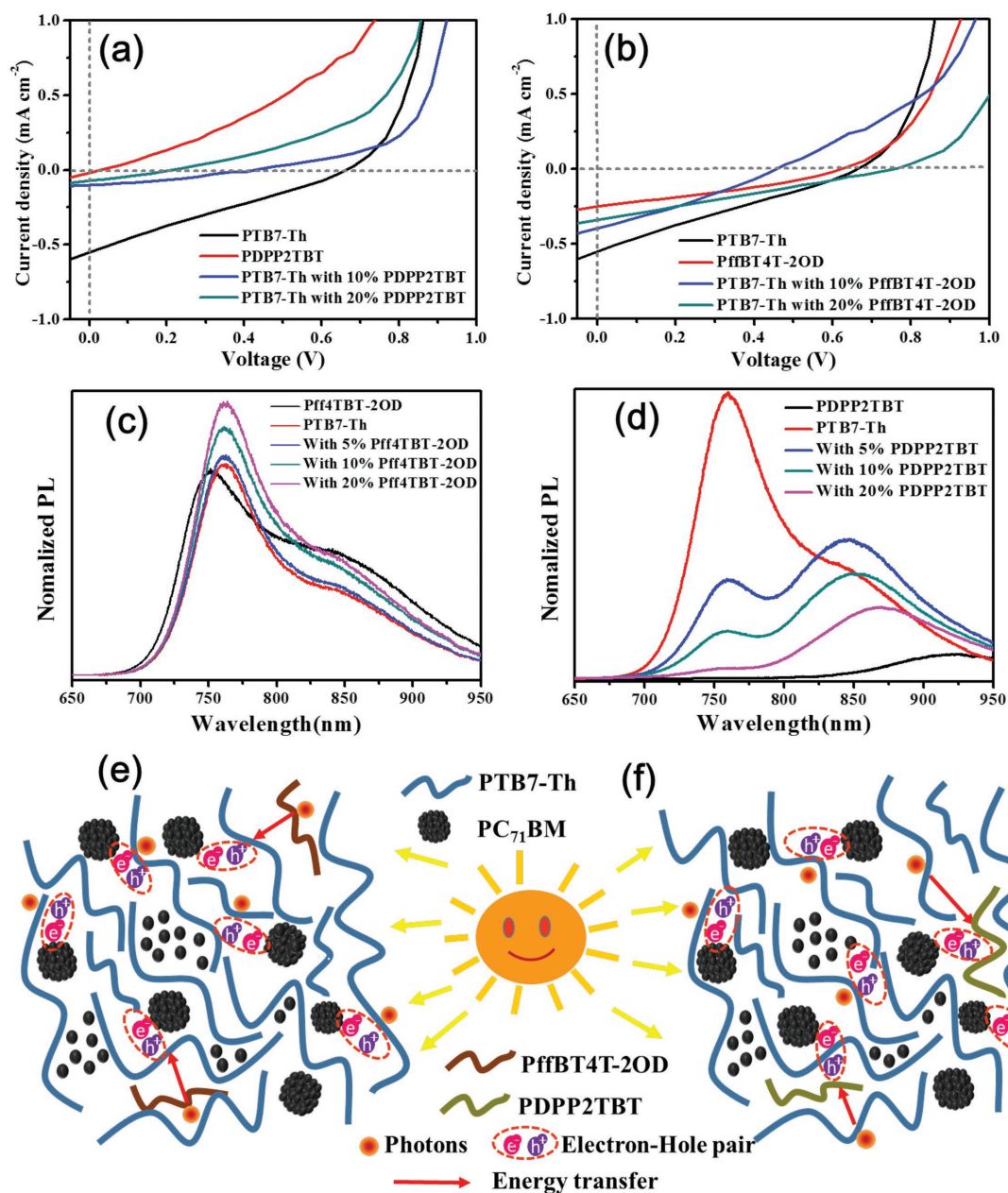


**Figure 4.** *J*-*V* curves of a) PTB7-Th:PDPP2TBT and b) PTB7-Th:PffBT4T-2OD binary solar cells with different blending ratios. PL spectra of PTB7-Th films with the addition of different amount of c) PffBT4T-2OD and d) PDPP2TBT. Scheme of energy transfer and charge dissociation in e) PffBT4T-2OD- and f) PDPP2TBT- based ternary system.

peaks of PffBT4T-2OD, PTB7-Th, and PDPP2TBT are located at 680, 700, and 850 nm, respectively, while the maximum PL emission peaks of them are located at 740, 760, and 920 nm, respectively, therefore energy transfer in these blends could in principle take place. From Figure 4c it can be seen that the relative PL intensity of PTB7-Th gradually increases upon blending with PffBT4T-2OD, while the PL of PffBT4T-2OD is quenched, implying energy transfer from PffBT4T-2OD to PTB7-Th. Within ternary blend OPVs we suggest that this process leads to an increase in the number of excited states on PTB7-Th which can undergo subsequent dissociation at the PTB7-Th:PC<sub>71</sub>BM interfaces (see Figure 4e), leading to improved photovoltaic per-

formance.<sup>[23]</sup> For the PTB7-Th:PDPP2TBT binary films, the relative PL intensity of PTB7-Th gradually decreases with increasing PDPP2TBT content. This produces a new PL spectrum with two primary peaks at 760 and 850–860 nm, respectively, which again is suggestive of energy transfer from PTB7-Th to PDPP2TBT (shown schematically in Figure 4f). As the offset between the LUMO levels of PDPP2TBT (−3.5 eV) and PC<sub>71</sub>BM (−4.0 eV) is only 0.5 eV, the energetic driving force for electron transfer between PDPP2TBT and PC<sub>71</sub>BM is relatively low, therefore energy that has been transferred from PTB7-Th to PDPP2TBT cannot be readily transferred into free charges. The weak EQE spectra in the wavelength range from 780 to 900 nm in Figure 1f



indicate that part of the photocurrent derives from PDPP2TB T:PC<sub>71</sub>BM;<sup>[37,38,55]</sup> however, the contribution of this cell is limited as the photocurrent generation between PDPP2TBT and PC<sub>71</sub>BM is inefficient, thus restricting the overall PCE of the PTB7-Th:PDPP2TBT:PC<sub>71</sub>BM ternary blend.

### 3. Conclusion

Two kinds of crystallizable, high hole mobility conjugated polymers, PffBT4T-2OD and PDPP2TBT, have been introduced into a PTB7-Th:PC<sub>71</sub>BM system as a second donor to fabricate ternary OPVs. These components demonstrated contrasting effects with improved efficiency in the PffBT4T-2OD-based ternary devices and reduced efficiency in the PDPP2TBT-based ternary OPVs, regardless of stronger complementary light absorption from the PDPP2TBT additive. A maximum PCE of 11% was achieved by adding 10% PffBT4T-2OD (relative to the polymer phase), mainly due to the increase  $J_{sc}$  and FF. Morphology studies suggest that the incorporation of PffBT4T-2OD and PDPP2TBT into the PTB7-Th:PC<sub>71</sub>BM blends obstructs the crystallization of these crystallizable additives, and both PffBT4T-2OD and PDPP2TBT were located in the PTB7-Th domains, increasing the average sizes of the phase-separated polymer and fullerene domains. In PffBT4T-2OD-based ternary OPVs, PffBT4T-2OD absorbs the light and transfers the energy to PTB7-Th, leading to an improved PCE. However, in the PDPP2TBT-based ternary OPVs, the energy absorbed by PTB7-Th will be partly transferred to PDPP2TBT, and the low-energy level offset between PDPP2TBT and PC<sub>71</sub>BM restricts device performance. Our results suggest that energy transfer is a critical factor that should be strongly considered when employing ternary photovoltaic blends strategy to improve device efficiency.

### 4. Experimental Section

**Materials:** PTB7-Th, PffBT4T-2OD, PDPP2TBT, and PC<sub>71</sub>BM were purchased from Solarmer Materials (Beijing) Inc. PEDOT:PSS (Clevios AI 4083) was purchased from Heraeus, Germany. TiO<sub>2</sub> nanoparticles were synthesized according to the previous report.<sup>[27]</sup> Unless otherwise stated, all chemicals and solvents were of reagent grade and used as received.

**Fabrication of Ternary Solar Cells:** Solar cells were fabricated with both conventional and inverted structures. The prepatterned ITO-glass substrates (resistance  $\approx 15 \Omega$  per square) were cleaned by sequential sonication in water, ethanol, and isopropyl alcohol for 10 min each, before drying at 100 °C on a hotplate. These substrates were further treated with ultraviolet/ozone for 10 min before solution processing. For the fabrication of conventional devices, 40 nm thick PEDOT:PSS films were spin-coated onto cleaned ITO substrates, then dried at 150 °C for 10 min in air. The active layer was then deposited on top of the PEDOT:PSS layer by spin-coating from a 14 mg mL<sup>-1</sup> chlorobenzene solution (with 3 vol% 1,8-diiodooctane (DIO)) of PTB7-Th: PffBT4T-2OD:PC<sub>71</sub>BM or PTB7-Th:PDPP2TBT:PC<sub>71</sub>BM to obtain films of 100 nm thickness, in a nitrogen-filled glove box. Then 5 nm Ca and 100 nm Ag were thermally evaporated onto the device under high vacuum, forming the cathode.

For the fabrication of inverted devices, 20 nm TiO<sub>2</sub>/TIPD films were cast from the TiO<sub>2</sub>/TIPD dispersion by spin-coating at 3000 rpm, followed by thermal annealing at 150 °C for 30 min to convert TiO<sub>2</sub>/TIPD to TiO<sub>2</sub>/TOPD. The films were then transferred into an N<sub>2</sub>-filled glove box and irradiated 10 min under a 254 nm UV light before rinsing with the ethanolamine solution (1 wt% in 2-methoxyethanol) at 3000 rpm.

The photoactive layer was spin-coated on TiO<sub>2</sub>/TOPD film with the same procedure as described above. Then 10 nm MoO<sub>3</sub> and 100 nm Ag were thermally evaporated forming an anode under high vacuum to finish the device preparation.

**Characterization:** Film absorption spectra were measured using a UV-visible Spectrophotometer (HITACHI, Japan). Film thickness was measured using a spectroscopic ellipsometer (J. A. Woollam, USA). Water contact angle measurements were performed using water contact angle measurement system (Attension Theta Lite), and the surface energy was calculated following the equation of state. The surface morphologies of the active layers were characterized by SPM (NT-MDT, Russia) and TEM (JEOL, Japan). Device  $J-V$  characterization was performed under AM1.5G (100 mW cm<sup>-2</sup>) using a Newport 3A solar simulator in air at room temperature. The light intensity was calibrated using a standard silicon reference cell certified by the National Renewable Energy Laboratory (USA).  $J-V$  characteristics were recorded using  $J-V$  sweep software developed by Ossila Ltd. (UK) and a Keithley (USA) 2612B source meter unit. An aperture mask was placed over the devices to accurately define a test area of 2.12 mm<sup>2</sup> on each pixel and to eliminate the influence of stray and wave guided light. EQE was measured with a Zolix (China) EQE system equipped with a standard Si diode. PL was obtained using a PL microscopic spectrometer (Flex One, Zolix, China) with a 532 nm continuous wave (CW) laser as the excitation source. Synchrotron GISAXS measurements were conducted using the beamline BL16B1 at the Shanghai Synchrotron Radiation Facility in China. Synchrotron GIWAXS measurements were conducted using the beamline IO7 at the Diamond Light Source in UK.

### Supporting Information

Supporting Information is available from the Wiley Online Library or from the author.

### Acknowledgements

This work was supported by the National Natural Science Foundation of China (Grants Nos. 21774097, 21504065) and the Fundamental Research Funds for the Central Universities (WUT: 2017-YB-010 and WUT: 2017IVA002) of China. T.W. acknowledges support from the Recruitment Program of Global Experts (1000 Talents Plan) of China. D.G.L. thanks the UK EPSRC for funding via grant EP/M025020/1 "High resolution mapping of performance and degradation mechanisms in printable photovoltaic devices." A.J.P. acknowledges support from the EPSRC through the grant EP/M024873/1 "Singlet Fission Photon Multipliers-Adding Efficiency to Silicon Solar Cells." All authors thank the beamline BL16B1 at Shanghai Synchrotron Radiation Facility (China) and the IO7 beamline at the Diamond Light Source (SI14701-1) for providing the beam time and help during experiments. We also thank Dr. Zhihong Chen (Department of Physics, Wuhan University of Technology) for helping with the GISAXS data analysis. The data underlying this publication are available at <https://doi.org/10.17863/CAM.13835>.

### Conflict of Interest

The authors declare no conflict of interest.

### Keywords

energy transfer, morphology, polymer solar cells, ternary solar cells

Received: July 26, 2017  
Revised: September 19, 2017  
Published online: December 4, 2017

- [1] L. Dou, J. You, Z. Hong, Z. Xu, G. Li, R. A. Street, Y. Yang, *Adv. Mater.* **2013**, 25, 6642.
- [2] C. B. Nielsen, S. Holliday, H. Y. Chen, S. J. Cryer, I. McCulloch, *Acc. Chem. Res.* **2015**, 48, 2803.
- [3] Y. Huang, E. J. Kramer, A. J. Heeger, G. C. Bazan, *Chem. Rev.* **2014**, 114, 7006.
- [4] J. Zhao, Y. Li, G. Yang, K. Jiang, H. Lin, H. Ade, W. Ma, H. Yan, *Nat. Energy* **2016**, 1, 15027.
- [5] Y. Yan, X. Liu, T. Wang, *Adv. Mater.* **2017**, 29, 1601674.
- [6] H. Ma, H. L. Yip, F. Huang, A. K. Y. Jen, *Adv. Funct. Mater.* **2010**, 20, 1371.
- [7] B. A. MacLeod, B. J. T. Villers, P. Schulz, P. F. Ndione, H. Kim, Z. Kai, S. R. Marder, S. Graham, J. J. Berry, A. Kahn, D. C. Olson, *Energy Environ. Sci.* **2015**, 8, 592.
- [8] W. Zhao, S. Li, H. Yao, S. Zhang, Y. Zhang, B. Yang, J. Hou, *J. Am. Chem. Soc.* **2017**, 139, 7148.
- [9] Y. Cui, H. F. Yao, B. Gao, Y. Qin, S. Zhang, B. Yang, C. He, B. Xu, J. Hou, *J. Am. Chem. Soc.* **2017**, 139, 7302.
- [10] H. Huang, L. Yang, B. Sharma, *J. Mater. Chem. A* **2017**, 5, 11501.
- [11] Y. Wang, W. D. Xu, J. D. Zhang, L. Zhou, G. Lei, C. F. Liu, W. Y. Lai, W. Huang, *J. Mater. Chem. A* **2017**, 5, 2460.
- [12] H. Bente, T. Nishida, D. Mori, H. Xu, H. Ohkita, S. Ito, *Energy Environ. Sci.* **2016**, 9, 135.
- [13] W. Zhao, S. Li, S. Zhang, X. Liu, J. Hou, *Adv. Mater.* **2017**, 29, 1604059.
- [14] T. Kumari, S. M. Lee, S. H. Kang, S. Chen, C. Yang, *Energy Environ. Sci.* **2017**, 10, 258.
- [15] H. Lu, X. Xu, Z. Bo, *Sci. China Mater.* **2016**, 59, 444.
- [16] W. Liu, S. Li, J. Huang, S. Yang, J. Chen, L. Zhao, M. Shi, X. Zhan, C. Z. Li, H. Chen, *Adv. Mater.* **2016**, 28, 9729.
- [17] Y. Qin, Y. Chen, Y. Cui, S. Zhang, H. Yao, J. Huang, W. Li, Z. Zhong, J. Hou, *Adv. Mater.* **2017**, 29, 1606340.
- [18] Y. Zhang, D. Deng, K. Lu, J. Zhang, B. Zhang, Y. Zhao, J. Fang, Z. Wei, *Adv. Mater.* **2015**, 27, 1071.
- [19] W. Su, Q. Fan, X. Guo, B. Guo, W. Li, Y. Zhang, M. Zhang, Y. Li, *J. Mater. Chem. A* **2016**, 4, 14752.
- [20] G. Zhang, K. Zhang, Q. Yin, X. F. Jiang, Z. Wang, J. Xin, W. Ma, H. Yang, F. Huang, Y. Cao, *J. Am. Chem. Soc.* **2017**, 139, 2387.
- [21] J. Zhang, Y. Zhang, J. Fang, K. Lu, Z. Wang, W. Ma, Z. Wei, *J. Am. Chem. Soc.* **2015**, 137, 8176.
- [22] N. Gasparini, X. Jiao, T. Heumueller, D. Baran, G. J. Matt, S. Fladischer, E. Spiecker, H. Ade, C. J. Brabec, T. Ameri, *Nat. Energy* **2016**, 1, 16118.
- [23] F. Zhao, Y. Li, Z. Wang, Y. Yang, Z. Wang, G. He, J. Zhang, L. Jiang, T. Wang, Z. Wei, W. Ma, B. Li, A. Xia, Y. Li, C. Wang, *Adv. Energy Mater.* **2017**, 7, 1602552.
- [24] Q. An, F. Zhang, J. Zhang, W. Tang, Z. Deng, B. Hu, *Energy Environ. Sci.* **2016**, 9, 281.
- [25] S. Liu, P. You, J. Li, C. S. Lee, B. S. Ong, C. Surya, F. Yan, *Energy Environ. Sci.* **2015**, 8, 1463.
- [26] Y. Chen, P. Ye, Z. G. Zhu, X. Wang, L. Yang, X. Xu, X. Wu, T. Dong, H. Zhao, J. Hou, F. Liu, H. Huang, *Adv. Mater.* **2017**, 6, 1603154.
- [27] Y. Yan, F. Cai, L. Yang, J. Li, Y. Zhang, F. Qin, C. Xiong, Y. Zhou, D. G. Lidzey, T. Wang, *Adv. Mater.* **2017**, 29, 1604044.
- [28] J. D. Chen, C. Cui, Y. Q. Li, L. Zhou, Q. D. Ou, C. Li, Y. Li, J. X. Tang, *Adv. Mater.* **2015**, 27, 1035.
- [29] F. Cai, L. Yang, Y. Yan, J. Zhang, F. Qin, D. Liu, Y. B. Chen, Y. Zhou, T. Wang, *J. Mater. Chem. A* **2017**, 5, 9402.
- [30] Z. He, B. Xiao, F. Liu, H. Wu, Y. Yang, S. Xiao, C. Wang, T. P. Russell, Y. Cao, *Nat. Photonics* **2015**, 9, 174.
- [31] Q. Wan, X. Guo, Z. Wang, W. Li, B. Guo, W. Ma, M. Zhang, Y. Li, *Adv. Funct. Mater.* **2016**, 26, 6635.
- [32] N. Gasparini, L. Lucera, M. Salvado, M. Prosa, G. D. Spyropoulos, P. Kubis, H. J. Egelhaaf, C. J. Brabec, T. Ameri, *Energy Environ. Sci.* **2017**, 10, 885.
- [33] T. Liu, L. Huo, X. Sun, B. Fan, Y. Cai, T. Kim, J. Y. Kim, H. Choi, Y. Sun, *Adv. Energy Mater.* **2016**, 6, 1502109.
- [34] Y. M. Yang, W. Chen, L. Dou, W. H. Chang, H. S. Duan, B. Bob, G. Li, Y. Yang, *Nat. Photonics* **2015**, 9, 190.
- [35] L. Yao, T. Xu, W. Chen, E. S. Landry, L. Yu, *Nat. Photonics* **2014**, 8, 716.
- [36] M. C. Scharber, D. Mühlbacher, M. Koppe, P. Denk, C. Waldauf, A. J. Heeger, C. J. Brabec, *Adv. Mater.* **2006**, 18, 789.
- [37] L. Lu, M. A. Kelly, W. You, L. Yu, *Nat. Photonics* **2015**, 9, 491.
- [38] P. P. Khlyabich, B. Burkhart, B. C. Thompson, *J. Am. Chem. Soc.* **2012**, 134, 9074.
- [39] T. H. Lee, M. A. Uddin, C. Zhong, S. J. Ko, B. Walker, T. Kim, Y. J. Yoon, S. Y. Park, A. J. Heeger, H. Y. Woo, J. Y. Kim, *Adv. Energy Mater.* **2016**, 6, 1600637.
- [40] Y. C. Chen, C. Y. Hsu, R. Y. Y. Lin, K. C. Ho, J. T. Lin, *ChemSusChem* **2013**, 6, 20.
- [41] R. A. Street, D. Davies, P. P. Khlyabich, B. Burkhart, B. C. Thompson, *J. Am. Chem. Soc.* **2013**, 135, 986.
- [42] Y. Liu, J. Zhao, Z. Li, C. Mu, W. Ma, H. Hu, K. Jiang, H. Lin, H. Ade, H. Yan, *Nat. Commun.* **2014**, 10, 5293.
- [43] J. Cho, S. H. Yu, D. S. Chung, *J. Mater. Chem. C* **2017**, 5, 2745.
- [44] F. Liu, W. Zhao, J. R. Tumbleston, C. Wang, Y. Cu, D. Wang, A. L. Briseno, H. Ade, T. P. Russell, *Adv. Energy Mater.* **2014**, 4, 1301377.
- [45] J. Mai, T. K. Lau, J. Li, S. H. Peng, C. S. Hsu, U. S. Jeng, J. Zeng, N. Zhao, X. Xiao, X. Lu, *Chem. Mater.* **2016**, 28, 6186.
- [46] H. J. Jhuo, S. H. Liao, Y. L. Li, P. N. Yeh, S. A. Chen, W. R. Wu, C. J. Su, J. J. Lee, N. L. Yamada, U. S. Jeng, *Adv. Funct. Mater.* **2016**, 26, 3094.
- [47] Y. J. Hsieh, Y. C. Huang, W. S. Liu, Y. A. Su, C. S. Tsao, S. P. Rwei, L. Wang, *ACS Appl. Mater. Interfaces* **2017**, 9, 14808.
- [48] P. Pfeifer, F. Ehrburger-Dolle, T. P. Rieker, M. T. González, P. Hoffman, M. Molina-Sabio, F. Rodríguez-Reinos, P. W. Schmidt, D. J. Voss, *Phys. Rev. Lett.* **2002**, 88, 115502.
- [49] S. Honda, H. Ohkita, H. Bente, S. Ito, *Adv. Energy Mater.* **2011**, 1, 588.
- [50] J. S. Huang, T. Goh, X. Li, M. Y. Sfeir, E. A. Bielinski, S. Tomasulo, M. L. Lee, N. Hazeri, A. D. Taylor, *Nat. Photonics* **2013**, 7, 479.
- [51] M. Zhang, F. Zhang, Q. An, Q. Sun, W. Wang, J. Zhang, W. Tang, *Nano Energy* **2016**, 22, 241.
- [52] W. Ma, G. Yang, K. Jiang, J. H. Carpenter, Y. Wu, X. Meng, T. McAfee, J. Zhao, C. Zhu, C. Wang, H. Ade, H. Yan, *Adv. Energy Mater.* **2015**, 5, 1501400.
- [53] L. Yang, L. Yan, W. You, *J. Phys. Chem. Lett.* **2013**, 4, 1802.
- [54] V. Gupta, V. Bharti, M. Kumar, S. Chand, A. L. Heeger, *Adv. Mater.* **2015**, 27, 4398.
- [55] H. Lu, J. Zhang, J. Chen, Q. Liu, X. Gong, S. Feng, X. Xu, W. Ma, Z. Bo, *Adv. Mater.* **2016**, 28, 9559.